# Room temperature operation of $In_xGa_{1-x}Sb$/InAs type-II quantum well infrared photodetectors grown by MOCVD

D. H. Wu, Y. Y. Zhang, and M. Razeghi

Citation: Appl. Phys. Lett. **112**, 111103 (2018); doi: 10.1063/1.5021646
View online: https://doi.org/10.1063/1.5021646
View Table of Contents: http://aip.scitation.org/toc/apl/112/11
Published by the American Institute of Physics

# Room temperature operation of $In_xGa_{1-x}Sb$/InAs type-II quantum well infrared photodetectors grown by MOCVD

D. H. Wu, Y. Y. Zhang, and M. Razeghi[a)]
*Center for Quantum Devices, Department of Electrical Engineering and Computer Science, Northwestern University, Evanston, Illinois 60208, USA*

(Received 6 January 2018; accepted 3 March 2018; published online 14 March 2018)

We demonstrate room temperature operation of $In_{0.5}Ga_{0.5}Sb$/InAs type-II quantum well photodetectors on an InAs substrate grown by metal-organic chemical vapor deposition. At 300 K, the detector exhibits a dark current density of 0.12 A/cm$^2$ and a peak responsivity of 0.72 A/W corresponding to a quantum efficiency of 23.3%, with the calculated specific detectivity of $2.4 \times 10^9$ cm Hz$^{1/2}$/W at 3.81 $\mu$m. *Published by AIP Publishing*. https://doi.org/10.1063/1.5021646

The mid-wavelength infrared (MWIR) window between 3 and 5 $\mu$m has wide applications from military to civilian,[1–3] such as aerial and satellite reconnaissance, target tracking using heat signals, navigation and object identification, vascular and cancer detection, and industrial process monitoring. For all these applications, achieving higher operating temperatures of a single element detector or imager is highly desirable because it will reduce the cost and complexity. During the past few years, tremendous effort has been spent on developing high operating temperature infrared photodetectors, most notably mercury-cadmium-telluride (MCT),[4] InAs/GaSb type-II superlattices (T2SLs),[5,6] and inter subband based quantum dot infrared photodetectors (QDIPs).[7] Although the state-of-the-art MWIR photodetectors based on a bulk MCT material have already demonstrated near-room temperature operation, the MCT material is still plagued by nonuniform growth and expensive CdZnTe substrates. InAs/GaSb-based T2SLs are viable candidates to compete with the state-of-the-art MCT material system due to their unique material characteristics, such as large effective mass and ability to suppress Auger recombination. High-performance MWIR photodetectors based on InAs/GaSb T2SLs have been extensively demonstrated.[8,9] However, most of the T2SL structures and devices have been grown by molecular beam epitaxy (MBE), which is expensive for mass production application due to the large costs of upkeep and very slow output rates. QDIPs utilize the intraband transitions for infrared detection. The quasi-three-dimensional confinement of the quantum dot (QD) provides important advantages for infrared photodetection such as inherent sensitivity to normal-incidence light, low dark current, and high operating temperature. Nevertheless, recently reported QDIP performances are still far below the theoretical expectation.[10,11] Recently, the Sb-based InSb/InAs type-II material system has attracted much interest in the MWIR band due to its unique type-II band alignment which can provide low-energy optical transitions in the III/V material system.[12,13] Although the InSb/InAs material system has a large mismatch (7%), similar to the well-known InAs/GaAs material system, Stranski–Krastanov (S-K) mode growth of InSb on InAs does not result in high quality QD due to the Sb segregation and surfactant effects.[14] Initial works on the growth of a thin InSb layer on InAs have demonstrated promising results in light-emitting diodes[15] and lasers.[16] More recently, efforts have been made to tune the strain and extend the emission wavelength by adding Gallium (Ga) to form an $In_xGa_{1-x}Sb$ thin layer on the InAs matrix for photodetector applications.[17,18] However, the photodetectors based on this material system are facing more challenges and therefore still have limited performance in recent reports.[17]

In this work, we report the growth of a high quality material and demonstration of high performance MWIR photodetectors based on $In_xGa_{1-x}Sb$/InAs type-II quantum well (QW) structures on an InAs substrate grown by metal-organic chemical vapor deposition (MOCVD), which could enable lower-cost and versatile production. Figure 1(a) shows a schematic of the device structure. For theoretical guidance, we applied the $\boldsymbol{k}\cdot\boldsymbol{p}$ model to calculate the bandstructure of the proposed type-II QW structure. Shown in Fig. 1(b) is the calculated type-II energy band diagram for the $In_{0.5}Ga_{0.5}Sb$/InAs QW associated with strain. In such $In_{0.5}Ga_{0.5}Sb$/InAs type-II QW structures, holes are confined in the $In_{0.5}Ga_{0.5}Sb$ well while electrons are not confined in the InAs barrier. The valence bands in the strained $In_{0.5}Ga_{0.5}Sb$ well are split into heavy- and light-hole bands. The detection mechanism is based on spatially indirect band to band transitions between the bound hole-states in the $In_{0.5}Ga_{0.5}Sb$ well and the continuous electron-states in the InAs barrier.

There are several advantages in this type of type-II QW photodetector. The first advantage resides in the suppression of the Auger recombination. Usually, Auger recombination is the dominant recombination mechanism at high temperatures and is one of the obstacles in realizing infrared detectors operating at high temperatures. The material systems with type-II band alignment such as $In_xGa_{1-x}Sb$/InAs superlattices, quantum wells, and quantum dots were recognized as promising materials for MWIR lasers and photodetectors due to the predicted reduced Auger recombination rates.[19–22] The proposed $In_{0.5}Ga_{0.5}Sb$/InAs type-II QW structures will apparently have a lower Auger recombination rate in comparison with type-I heterostructures and bulk materials due to their type-II band alignment. Another promising advantage is the long carrier lifetime. The lifetime of minority carriers is an important parameter which defines both the dark

a)Electronic mail: razeghi@eecs.northwestern.edu

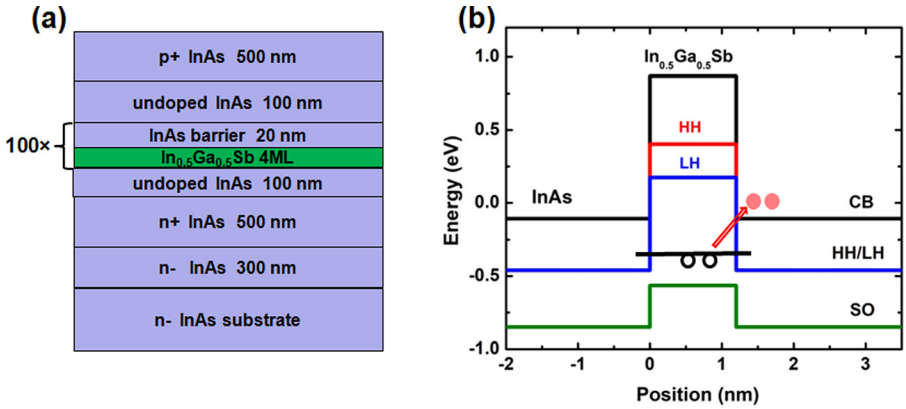


FIG. 1. (a) Schematic layer design of the $In_{0.5}Ga_{0.5}Sb$/InAs type-II QW photodiode; (b) schematic energy band diagram of $In_{0.5}Ga_{0.5}Sb$ QW with the InAs barrier.

current and quantum efficiency (QE) of photodetectors. In $In_xGa_{1-x}Sb$/InAs type-II QW structures, electrons in the InAs barrier and holes in the $In_xGa_{1-x}Sb$ well are separated compared to those in conventional type-I structures. The spatially indirect nature of the transitions is beneficial for a long carrier lifetime.[23,24]

The device was grown on an n-type InAs substrate in an EMCORE MOCVD reactor at a pressure of 60 Torr. Trimethylindium (TMIn) and triethylgallium (TEGa) were used as group III precursors. Trimethylantimony (TMSb) and $AsH_3$ were used as group V precursors. Diethylzinc (DEZn) and $SiH_4$ were used for p-type and n-type dopants, respectively. The growth of the device structure started with a 300 nm n-type InAs buffer layer to smooth out the surface. Then, a 0.5 $\mu$m n-type ($n \sim 10^{18}\,cm^{-3}$) InAs bottom contact was grown, which was followed by the 100 period undoped $In_{0.5}Ga_{0.5}Sb$/InAs type II QW active region and a 0.5 $\mu$m thick p-type ($p \sim 10^{18}\,cm^{-3}$) InAs top contact. The $In_{0.5}Ga_{0.5}Sb$ well layer was grown with a nominal thickness of 4 ML separated by a 20 nm InAs barrier. The whole structure was grown at 430 °C. After the growth, the sample was structurally characterized using high resolution X-ray diffraction (HR-XRD), atomic force microscopy (AFM), and transmission electron microscopy (TEM).

Figure 2 shows the X-ray diffraction scan curve (a), AFM image (b), and TEM (c) characterization results of the grown device structure. In the XRD curve, satellite peaks up to 7th-order are clearly observed, which indicates an excellent structural quality. The full width at half maximum (FWHM) values at 0th and 1st satellite peaks are only 30 and 54 arc sec, respectively. The overall period is 20.1 nm, which is in good agreement with the designed value. The lattice mismatch between the InAs substrate and the active region is 1556 ppm. The sample exhibits a good surface morphology with clear atomic steps. The root mean square (RMS) roughness is only 1.1 Å for the $5 \times 5\,\mu m^2$ scan area. Figure 2(c) is the cross-sectional dark-field TEM image of a representative portion of the active region in our device using the (002) reflection. The $In_{0.5}Ga_{0.5}Sb$ layer looks like an ultrathin planar layer and shows no evidence of defect. The XRD, AFM, and TEM results suggest excellent material quality for our detector device.

The material was subsequently processed into mesa isolated single element diodes with device sizes ranging from $100 \times 100$ to $400 \times 400\,\mu m^2$ using a standard photolithographic processing technique followed by mesa definition using BCl3:Ar+ dry etching and citric acid treatment to remove dry etch residues. Top and bottom metal contacts were formed using electron beam deposited Ti/Au. Then, the devices were wire-bonded onto a 68 pin leadless chip carrier (LCCC) and loaded into a cryostat for both optical and electrical characterizations in the temperature range from 150 to 300 K.

The device was optically characterized under front-side illumination without any anti-reflection (AR) coating applied to the devices. The spectral response was measured using a Bruker IFS 66v/S Fourier transform infrared spectrometer (FTIR), and the responsivity ($R_i$) and quantum efficiency (QE) were measured with a calibrated blackbody source at 1000 °C. The device shows zero bias dependent performance. The $R_i$ and QE spectra of the device measured at zero bias are shown in Figs. 3(a) and 3(b) for temperatures of 150 and 300 K. As we can see, there are two distinctly different photoresponses in the spectra. The short wavelength photoresponse

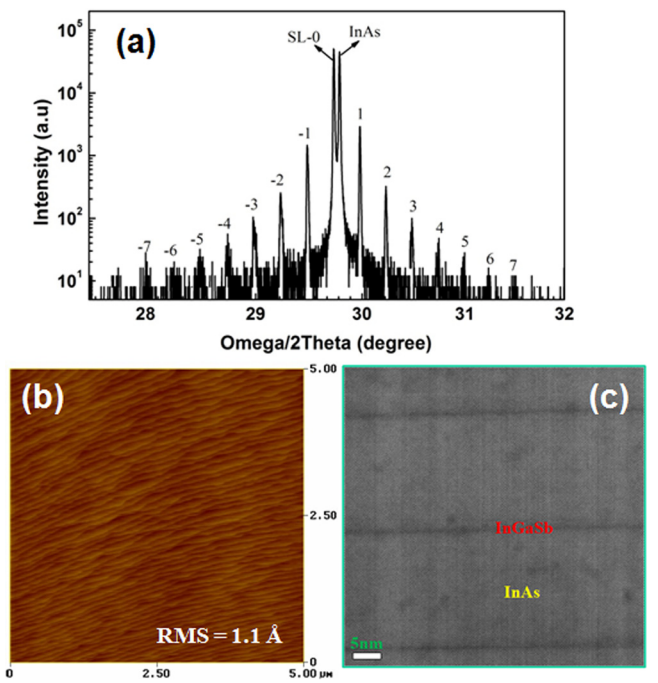


FIG. 2. (a) High-resolution X-ray diffraction of the grown device structure; (b) the atomic force microscopy image of a $5 \times 5\,\mu m^2$ surface area of the grown device structure with a RMS roughness value of 1.1 Å; (c) DF-TEM image of $In_{0.5}Ga_{0.5}Sb$/InAs QW in the grown device structure.

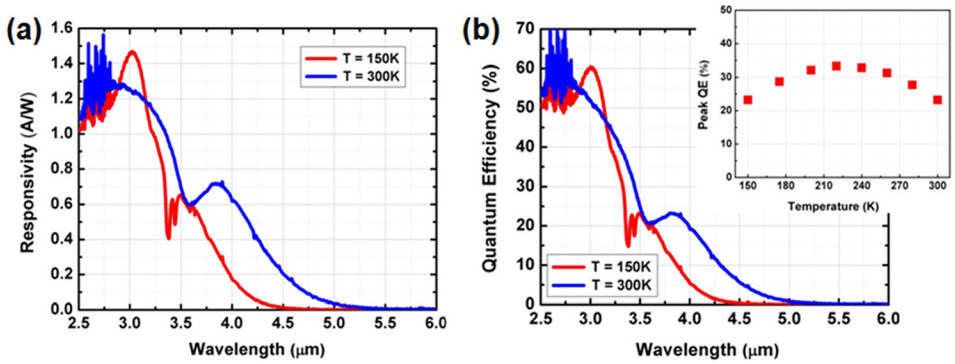


FIG. 3. (a) Responsivity spectra and (b) quantum efficiency spectra of the photodetector under zero bias at 150 and 300 K. Inset of (b): The peak quantum efficiency value of the photoresponse from InGaSb/InAs Type-II QW from 150 to 300 K.

with an approximate 3.5 $\mu$m cut-off originates from the direct bandgap transitions in the InAs barrier material,[24] while the photoresponse with an approximate 5.0 $\mu$m cut-off is due to the type-II transitions from the bound hole states in the $In_{0.5}Ga_{0.5}Sb$ well to the conduction band states in the InAs barrier.

The photodetectors exhibit a 100% cut-off wavelength of ~4.50 $\mu$m at 150 K; the responsivity peaks at 0.65 A/W, corresponding to a QE of 23.2% at 3.48 $\mu$m for the 100 period $In_{0.5}Ga_{0.5}Sb$/InAs type-II QW active region. At 300 K, the detector shows a 100% cut-off wavelength of ~5.22 $\mu$m; the peak responsivity is 0.72 A/W at 3.81 $\mu$m, corresponding to a QE of 23.3%. The temperature dependent optical performance of the device was also characterized. The inset of Fig. 3(b) shows the peak QE value of the photoresponse from type-II QW at the peak responsivity wavelength from 150 to 300 K. The type-II QW related photoresponse QE increases gradually with temperature, and the highest QE of 33.4% is obtained around 220 K. For temperature above 220 K, the QE starts to decrease. In a p-i-n photodiode, QE is determined primarily by the absorption coefficient of the material and diffusion length of minority carriers. For the $In_{0.5}Ga_{0.5}Sb$/InAs type-II QW device structure, the absorption coefficient increases with increasing temperature. This leads to an increase in QE when temperature increases from 150 to 220 K. With the temperature increased to 200 K above, the minority carrier lifetime starts to decrease due to the stronger Auger recombination. This will result in the decrease in the minority carrier diffusion length, which is the main reason for decreased QE at high temperature.

For the temperature dependent electrical performance measurement, a cold shield was placed in front of the photodetectors. Figure 4(a) exhibits the dark current density as a function of the applied bias voltage at different temperatures from 150 to 300 K. At 150 K and −20 mV bias, the photodetector shows a dark current density and differential resistance × area (R × A) product of $1.5 \times 10^{-7}$ A/cm$^2$ and 200 876 Ω cm$^2$, respectively. At 300 K, the dark current density and R × A product at −20 mV bias are 0.12 A/cm$^2$ and 0.2 Ω cm$^2$, respectively. An Arrhenius plot of the dark current density versus the inverse temperature (1/T) from 150 to 300 K under −20 mV applied bias voltage is shown in Fig. 4(b). An activation energy of about 340 meV was obtained, which corresponded roughly to the InAs bandgap (350 meV). This indicates that the dark current is diffusion current limited assisted via the InAs barrier.

After the electrical and optical characterization of the device, the specific detectivity ($D^*$) was calculated using the following equation:

$$D^* = R_i \left[ 2qJ + \frac{4k_bT}{R \times A} \right]^{-1/2}, \quad (1)$$

where q is the electronic charge, $k_b$ is Boltzmann's constant, and $T$ is the temperature of the device. Shown in Fig. 5 are the calculated specific detectivity ($D^*$) of the device based on the measured responsivity, the dark current density, and the R × A product at different temperatures under −20 mV applied bias. At 150 K, a peak detectivity $D^*$ of $6.2 \times 10^{11}$ cm Hz$^{1/2}$/W was calculated at peak responsivity ($\lambda = 3.48$ $\mu$m) and the device exhibited a peak detectivity $D^*$ of $2.4 \times 10^9$ cm Hz$^{1/2}$/W at peak responsivity ($\lambda = 3.81$ $\mu$m) at 300 K. The $In_{0.5}Ga_{0.5}Sb$/InAs type-II QW MWIR detectors have demonstrated excellent electrical and optical performance at room temperature.

In conclusion, we reported an $In_{0.5}Ga_{0.5}Sb$/InAs type-II QW MWIR photodetector grown on an InAs substrate by MOCVD. The detector shows a peak responsivity of 0.65 A/W at the wavelength of 3.48 $\mu$m and a dark current density of $1.5 \times 10^{-7}$ A/cm$^2$, with the calculated specific detectivity of $6.2 \times 10^{11}$ cm Hz$^{1/2}$/W at 150 K. At 300 K, the peak responsivity is 0.72 W/A at 3.81 $\mu$m and the dark current density is 0.12 A/cm$^2$, with the calculated specific detectivity of $2.4 \times 10^9$ cm Hz$^{1/2}$/W. Our results suggest great potential for the realization of high performance MWIR

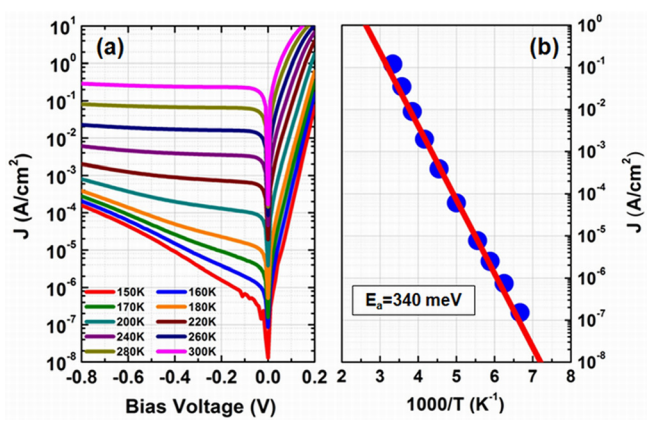


FIG. 4. (a) Dark current density as a function of applied bias voltage measured at different temperatures from 150 to 300 K; (b) Arrhenius plot of the dark current density of the detector under −20 mV applied bias.

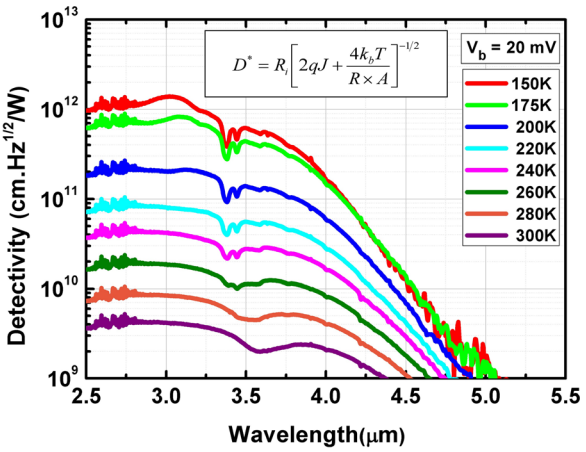


FIG. 5. Specific detectivity ($D^*$) spectra of the detector under −20 mV applied bias at different temperatures from 150 to 300 K.

photodetectors based on the $In_{0.5}Ga_{0.5}Sb$/InAs type-II QW structure on the InAs substrate.

The authors would like to acknowledge Dr. Yaobin Xu and Professor Vinayak P. Dravid from the Department of Materials Science and Engineering at Northwestern University for the TEM measurement.

[1]J. W. Beletic, R. Blank, D. Gulbransen, D. Lee, M. Loose, E. C. Piquette, T. Sprafke, W. E. Tennant, M. Zandian, and J. Zino, "Teledyne imaging sensor: Infrared imaging technologies for astronomy and civil space," in *Infrared SPIE Paper* (2008), p. 7021-20.
[2]R. D. Gehrza, E. E. Becklinb, I. de Paterc, D. F. Lesterd, T. L. Roellige, and C. E. Woodward, "A new window on the cosmos: The stratospheric observatory for infrared astronomy (SOFIA)," Adv. Space Res. **44**, 413 (2009).
[3]E. F. Ring and K. Ammer, "Infrared thermal imaging in medicine," Physiol. Meas. **33**, R33 (2012).
[4]M. A. Kinch, "HgCdTe: Recent trends in the ultimate IR semiconductor," J. Electron. Mater. **39**, 1043 (2010).
[5]M. Razeghi, "Focal plane arrays in type-II superlattices," U.S. patent 6,864,552 (2005).
[6]A. Rogalski, P. Martyniuk, and M. Kopytko, "InAs/GaSb type-II superlattice infrared detectors: Future prospect," Appl. Phys. Rev. **4**, 031304 (2017).
[7]P. Martyniuk and A. Rogalski, "Quantum-dot infrared photodetectors: Status and outlook," Prog. Quantum Electron. **32**, 89 (2008).
[8]Y. Wei, A. Hood, H. Yau, A. Gin, M. Razeghi, M. Z. Tidrow, and V. Nathan, "Uncooled operation of type-II InAs/GaSb superlattice photodiodes in the mid wavelength infrared range," Appl. Phys. Lett. **86**, 233106 (2005).
[9]J. V. Li, C. J. Hill, J. Mumolo, S. Gunapala, S. Mou, and S. L. Chuang, "Mid infrared type-II InAs/GaSb superlattice photodiodes toward room temperature operation," Appl. Phys. Lett. **93**, 163505 (2008).
[10]S. Tsao, H. Lim, W. Zhang, and M. Razeghi, "High operating temperature 320 × 256 middle-wavelength infrared focal plane array imaging based on an InAs/InGaAs/InAlAs/InP quantum dot infrared photodetector," Appl. Phys. Lett. **90**, 201109 (2007).
[11]A. V. Barve, J. Montaya, Y. Sharma, T. Rotter, J. Shao, W.-Y. Jang, S. Meesala, S. J. Lee, and S. Krishna, "High temperature operation of quantum dots-in-a-well infrared photodetectors," Infrared Phys. Technol. **54**, 215 (2011).
[12]V. A. Solov'ev, O. G. Lyublinskaya, A. N. Semenov, B. Y. Meltser, D. D. Solnyshkov, Y. V. Terent'ev, L. A. Prokopova, A. A. Toropov, S. V. Ivanov, and P. S. Kop'ev, "Room-temperature 3.9-4.3 μm photoluminescence from InSb submonolayers grown by molecular beam epitaxy in an InAs matrix," Appl. Phys. Lett. **86**, 011109 (2005).
[13]G. H. Yeap, S. I. Rybchenko, I. E. Itskevich, and S. K. Haywood, "Type-II $InAs_xSb_{1-x}$/InAs quantum dots for mid infrared applications: Effect of morphology and composition on electronic and optical properties," Phys. Rev. B **79**, 075305 (2009).
[14]A. Semenov, O. G. Lyublinskaya, V. A. Solov'ev, B. Y. Meltser, and S. V. Ivanov, "Surface segregation of Sb atoms during molecular-beam epitaxy of InSb quantum dots in an InAs(Sb) matrix," J. Cryst. Growth **301–302**, 58 (2007).
[15]P. J. Carrington, V. A. Solov'ev, Q. Zhuang, A. Krier, and S. V. Ivanov, "Room temperature midinfrared electroluminescence from InSb/InAs quantum dot light emitting diodes," Appl. Phys. Lett. **93**, 091101 (2008).
[16]Q. Lu, Q. Zhuang, J. Hayton, M. Yin, and A. Krier, "Gain and tuning characteristics of mid-infrared InSb quantum dot diode lasers," Appl. Phys. Lett. **105**, 031115 (2014).
[17]O. Gustafsson, A. Karim, C. Asplund, Q. Wang, T. Zabel, S. Almqvist, S. Savage, J. Y. Andersson, and M. Hammar, "A performance assessment of type-II interband $In_{0.5}Ga_{0.5}Sb$ QD photodetectors," Infrared Phys. Technol. **61**, 319 (2013).
[18]R. Liu, Y. Zhong, L. Yu, H. Kim, S. Law, J.-M. Zuo, and D. Wasserman, "Mid-infrared emission from In(Ga)Sb layers on InAs(Sb)," Opt. Express **22**, 24466 (2014).
[19]E. R. Youngdale, J. R. Meyer, C. A. Hoffman, F. J. Bartoli, C. H. Grein, P. M. Young, H. Ehrenreich, R. H. Miles, and D. H. Chow, "Auger lifetime enhancement in InAs-$Ga_{1-x}In_xSb$ superlattices," Appl. Phys. Lett **64**, 3160 (1994).
[20]G. G. Zegrya and A. D. Andreev, "Mechanism of suppression of Auger recombination processes in type-II heterostructures," Appl. Phys. Lett. **67**, 2681 (1995).
[21]J. R. Meyer, C. L. Felix, W. W. Bewley, I. Vurgaftman, E. H. Aifer, L. J. Olafsen, J. R. Lindle, C. A. Hoffman, M.-J. Yang, B. R. Bennett, B. V. Shanabrook, H. Lee, C.-H. Lin, S. S. Pei, and R. H. Miles, "Auger coefficients in type-II InAs/$Ga_{1-x}In_xSb$ quantum wells," Appl. Phys. Lett. **73**, 2857 (1998).
[22]T. Zabel, C. Reuterskiöld Hedlund, O. Gustafsson, A. Karim, J. Bereggren, Q. Wang, C. Ernerheim-Jokumsen, M. Soldemo, J. Weissenrieder, M. Götelid, and M. Hammar, "Auger recombination in In(Ga)Sb/InAs quantum dots," Appl. Phys. Lett. **106**, 013103 (2015).
[23]Y. D. Jang, T. J. Badcock, D. J. Mowbray, M. S. Skolnick, J. Park, D. Lee, H. Y. Liu, M. J. Steer, and M. Hopkinson, "Carrier lifetimes in type-II InAs quantum dots capped with a GaAsSb strain reducing layer," Appl. Phys. Lett. **92**, 251905 (2008).
[24]K. Nishikawa, Y. Takeda, T. Motohiro, D. Sato, J. Ota, N. Miyashita, and Y. Okada, "Extremely long carrier lifetime over 200 ns in GaAs wall-inserted type II InAs quantum dots," Appl. Phys. Lett. **100**, 113105 (2012).